JOURNAL OF THERMOPHYSICS AND HEAT TRANSFER
Vol. 21, No. 1, January–March 2007

Accurate Molecular and Soot Infrared Radiation Model for High-Temperature Flows

T. Ozawa, M. B. Garrison, and D. A. Levin
Pennsylvania State University, University Park, Pennsylvania 16802-1441

DOI: 10.2514/1.19137

The accurate computation of infrared spectral radiation from high-temperature, nonequilibrium flows remains a challenging problem, particularly for polyatomic species and particulates. A versatile computer model for calculating the infrared radiation of water and carbon dioxide and soot in generic flowfields is proposed and examined. Molecular radiation is calculated using the high-resolution transmission absorption molecular database/high-temperature spectroscopic absorption parameters and carbon dioxide spectroscopic databank-1000 line-by-line databases to provide high-resolution, accurate spectra between 200 and 8200 cm^{-1}. Soot particulate radiation is modeled using the first-term approximation of Mie scattering theory, and the pseudogas approximation is used. The program was parallelized in spectral increments to run efficiently on a message-passing interface equipped cluster. Validation was performed against well-documented radiation models such as ATHENA and nonequilibrium air radiation—infrared. Soot radiative properties were validated against measurements made on a sooting diffuse laminar flame, and carbon dioxide spectra were validated against experimental data. The computer radiation model is applied to two situations: a nonequilibrium bow shock and an Atlas-like sooting plume.

Nomenclature

a_i	=	ith a coefficient from Mie theory
B	=	first rotational energy constant, cm^{-1}
$B_\eta(T)$	=	radiative source function, $\mathrm{W/cm^2 \cdot sr \cdot cm^{-1}}$
b_i	=	ith b coefficient from Mie theory
D	=	second rotational energy constant, cm^{-1}
E_l	=	lower state energy, cm^{-1}
E_η	=	integrated intensity of a transition, $\mathrm{W/cm^3 \cdot sr}$
$F(J)$	=	rotational energy at the rotational state J, cm^{-1}
$G(v_1, v_2, v_3)$	=	vibrational energy at the vibrational state (v_1, v_2, v_3), cm^{-1}
g_l	=	lower state degeneracy
g_u	=	upper state degeneracy
I_a	=	isotopic abundance
I_i	=	molecular moment of inertia
J_l	=	lower state rotational quantum number
J_u	=	upper state rotational quantum number
k_η	=	spectral absorption coefficient, $\mathrm{cm}^{-1}/(\mathrm{molecule \cdot cm^{-2}})$
l	=	length of a gas element, cm
m	=	complex index of refraction of a particle, in the form $n - ik$
N	=	number density of gas in an element, $\mathrm{molecule/cm^3}$
P	=	pressure, atm
P_p	=	partial pressure, atm
$Q(T)$	=	internal partition sum at temperature T
Q_{abs}	=	dimensionless absorption efficiency of a particle
Q_{ext}	=	dimensionless extinction efficiency of a particle
$Q_{\mathrm{rot}}(T_{\mathrm{rot}})$	=	rotational partition sum at a temperature T_{rot}
Q_{scat}	=	dimensionless scattering efficiency of a particle
$Q_{\mathrm{vib}}(T_{\mathrm{vib}})$	=	vibrational partition sum at a temperature T_{vib}
$q_{v_l v_u}$	=	Franck–Condon factor from NEQAIR
$\lvert R_e(r_{v_l v_u})\rvert^2$	=	squared transition moment from NEQAIR, D^2
$R_{\eta,\mathrm{in}}$	=	spectral radiance incident on a gas element, $\mathrm{W/(cm^2 \cdot sr \cdot cm^{-1})}$
$R_{\eta,\mathrm{out}}$	=	spectral radiance exiting a gas element, $\mathrm{W/(cm^2 \cdot sr \cdot cm^{-1})}$
$\mathcal{R}_{lu}$	=	weighted transition moment squared from HITRAN, D^2
S	=	line intensity factor from Eq. (15)
$S_\eta(T)$	=	line strength at temperature T, $\mathrm{W/(cm^2 \cdot sr \cdot cm^{-1})}$
T	=	temperature, K
T_{ref}	=	reference temperature of a spectroscopic database, K
T_{rot}	=	rotational temperature, K
T_{trans}	=	translational temperature, K
T_{vib}	=	vibrational temperature, K
v_{il}	=	lower state vibrational quantum number of the ith mode
v_{iu}	=	upper state vibrational quantum number of the ith mode
x	=	dimensionless parameter from Mie theory
x_{ij}	=	vibrational constant for the ith and jth modes, cm^{-1}
γ_D	=	Doppler half-width at half-maximum, cm^{-1}
γ_L	=	Lorentz half-width at half-maximum, cm^{-1}
η	=	wave number, cm^{-1}
η^*	=	pressure-shifted wave number, cm^{-1}
η_o	=	central wave number for a transition, cm^{-1}
σ	=	rotational degeneracy
τ	=	spectral transmissivity
ω_i	=	vibrational constant for the ith mode, cm^{-1}

Presented as Paper 4777 at the 36th AIAA Plasmadynamics and Lasers Conference, Toronto, ON, Canada, 6–9 June 2005; received 26 July 2005; revision received 16 February 2006; accepted for publication 18 February 2006.

I. Introduction

OVER the past few decades, the study of accurate infrared molecular radiation has led to the generation of a variety of specialized computer models. Usually intended for modeling furnace combustion or atmospheric propagation, these models are typically limited to a combination of low-temperature, high-pressure, and local thermal equilibrium (LTE) conditions. Models [1,2] that are free of those restrictions are often incomplete, lacking such vital IR radiators as carbon dioxide and water vapor at high temperatures. Moreover, these limited conditions fail to describe the study of radiation from within a supersonic shock layer. Such flowfields exhibit both low- and midrange pressures necessitating the use of a

versatile Voigt line shape as well as temperatures that range from 200–6,000 K. More important, because of the low number density, high gas velocity, and thin shock layer, these flows are often in a state of nonlocal thermal equilibrium (non-LTE).

In response to this need, a new, high-fidelity computer model, designated as the nonequilibrium radiation distribution (NERD) program, has been developed in this work to model the high-temperature IR radiation for CO_2 and H_2O for a wide variety of conditions. It is intended to be used with a program such as nonequilibrium air radiation—infrared (NEQAIR-IR) [3], which only includes diatomic molecules and atoms. The NERD program uses input from the high-temperature spectroscopic absorption parameters database (HITEMP) [4] and the carbon dioxide spectroscopic databank (CDSD-1000) [5] spectral databases to calculate the transmissivity, radiance ($W/cm^2 \cdot sr \cdot cm^{-1}$) and integrated intensity ($W/cm^2 \cdot sr$) for a heterogeneous line of sight (LOS) with vibrational temperatures in excess of 2000 K. Voigt line shapes are used to cover the range of pressures and temperatures expected in hypersonic flows, and the use of separate molecular partition functions for each of the internal energy modes (vibrational and rotational) allows for the calculation of non-LTE conditions.

In addition to the high-temperature nonequilibrium characteristics of hypersonic radiation, spectra can be complicated by the presence of particulates in two-phase flows. Depending on the size and concentrations, these particulates can significantly affect the magnitude and spectral distribution of the radiation. Hence to provide a more complete radiation model, particulate radiation is also included. For the conditions of this work, because the particle size is small compared to the wavelengths of interest, the pseudogas approximation, which neglects scattering, is used.

The HITEMP [4] database, which is the high-temperature equivalent of the high-resolution transmission absorption molecular database (HITRAN), is a line-by-line database of absorption data for CO, CO_2, and H_2O. HITEMP has information on thousands to millions of spectral lines per molecule, including line positions, intensities, air- and self-broadened half-widths, and coefficients of temperature and pressure dependences. For each line, the position, intensity, and half-width values are scaled to a reference condition of 296 K and 1 atm. Three different data files, calibrated for different maximum temperatures, are used to calculate line positions and intensities for H_2O in NERD.

However, a better alternative exists for the calculation of the high-temperature spectral properties for CO_2. The CDSD-1000 [5] is an extensive database of 3×10^6 carbon dioxide absorption lines. The data file is in the same format as the HITEMP databases, making it easy to switch between the two. It has been shown through past work [5] that this database is more accurate than its counterpart for the high temperatures encountered in a shock layer.

In the paper we discuss the theory and implementation and validation of the NERD model and provide two example applications. In Sec. II we discuss the relevant theory necessary to use the database of line strengths, established by Rothman [4], the particulate radiation model, the equations relevant to radiative transport, and the parallel computer implementation that takes advantage of multiprocessor Beowulf clusters. Section III presents validation of NERD against established and widely used models such as ATHENA [2] and NEQAIR-IR [3]. These models were chosen because ATHENA, although an equilibrium, band model, uses high-temperature molecular properties. Additional validation of the high-temperature carbon monoxide spectra predicted by NEQAIR-IR ensures that NERD has correctly modeled molecular nonequilibrium transitions. In this section, we also discuss validation of NERD with the experimental carbon dioxide spectra and particulate radiation. Finally, in Sec. IV we present two applications of the NERD model: radiation from a hypersonic blow shock and a lox-kerosene plume.

II. Theory and Implementation

The NERD code calculates radiance and intensity for a one-dimensional line of sight through the given flowfield. The large gradients found in shock flowfields lead to large inaccuracies when using the Curtis–Godson approximation [6]. Instead, NERD treats each LOS as a consecutive row of finite gas elements, with all parameters constant across an element. These LOS can be taken directly from a typical CFD solution and can thus be adjusted to capture any details of the flowfield.

Line strengths were calculated from the HITEMP database for H_2O and from the CDSD-1000 database for CO_2 using the method outlined by Rothman [4]. To allow separation of the rotational and vibrational states, the temperature ratios of the lower state energy E_l and transition wave number η must be divided as follows:

$$\frac{E_l}{T} = \frac{F(J_l)}{T_{\text{rot}}} + \frac{G(v_{1l}, v_{2l}, v_{3l})}{T_{\text{vib}}} \tag{1}$$

$$\frac{\eta}{T} = \frac{F(J_u) - F(J_l)}{T_{\text{rot}}} + \frac{G(v_{1u}, v_{2u}, v_{3u}) - G(v_{1l}, v_{2l}, v_{3l})}{T_{\text{vib}}} \tag{2}$$

where the values $F(J)$ and $G(v_1, v_2, v_3)$ are defined by Herzberg [7].

$$F(J) = BJ(J+1) - D[J(J+1)]^2 \tag{3}$$

$$\begin{aligned} G(v_1, v_2, v_3) = {} & \omega_1(v_1 + \tfrac{1}{2}) + \omega_2(v_2 + \tfrac{1}{2}) + \omega_3(v_3 + \tfrac{1}{2}) + x_{11}(v_1 \\ & + \tfrac{1}{2})^2 + x_{22}(v_2 + \tfrac{1}{2})^2 + x_{33}(v_3 + \tfrac{1}{2})^2 + x_{12}(v_1 + \tfrac{1}{2})(v_2 + \tfrac{1}{2}) \\ & + x_{23}(v_2 + \tfrac{1}{2})(v_3 + \tfrac{1}{2}) + x_{13}(v_1 + \tfrac{1}{2})(v_3 + \tfrac{1}{2}) \end{aligned} \tag{4}$$

The internal partition function Q is split into its vibrational and rotational components [8]

$$Q_{\text{rot}}(T_{\text{rot}}) = \frac{1}{\sigma} \prod_{i=x,y,z} \sqrt{\frac{2I_i k T_{\text{rot}}}{\hbar^2}} \tag{5}$$

$$Q_{\text{vib}}(T_{\text{vib}}) = \prod_i (1 - \exp^{\frac{-hc\eta_i}{kT_{\text{vib}}}})^{g_i} \tag{6}$$

where σ is the symmetry of the molecule.

The HITEMP, HITRAN, and CDSD-1000 databases have reference values for the air- and self-broadened half-width at half-maximum, γ_{air} and γ_{self}, and a temperature dependence term n. The Doppler and Lorentz half-widths can then be found by using relationships from Ludwig [6] and Rothman [4], respectively.

Particle radiation capabilities have been incorporated into the NERD code to model the soot contribution to the flowfield infrared radiation. Mie theory predicts the scattering and absorption of a particle based on the nondimensional parameter x, defined as the ratio of the particle circumference and the wavelength of incident light [9]. The present maximum wave number that can be modeled by NERD is 8310 cm^{-1}, which corresponds with the upper bound of data given by the CDSD-1000 database. Assuming a maximum soot radius of 25 nm [10,11], in this wavelength domain $x < 0.1$, and scattering accounts for less than 0.5% of the extincted photons. It is therefore safe to treat particle radiation with the pseudogas assumption, that is, particles can emit and absorb radiation but cannot scatter it. This simplifies the calculations and preserves the one dimensionality of the LOS calculations in NERD. In addition, at this low x value, the first Mie coefficients, a_1 and b_1, account for over 99% of the scattering and absorption efficiencies, leading to the simpler first-term approximation. This gives a direct solution for a_1 and b_1 and differs from the full expression by less than 3% in the domain considered here [12]. Equations (7–9) give expressions for the Mie efficiencies using the first-term approximation.

$$Q_{\text{ext}} = \frac{6}{x^2} Re(a_1 + b_1) \tag{7}$$

$$Q_{\text{scat}} = \frac{6}{x^2} Re(|a_1|^2 + |b_1|^2) \tag{8}$$

$$Q_{\text{abs}} = Q_{\text{ext}} - Q_{\text{scat}} \tag{9}$$

and the absorption coefficient k is related to the absorption efficiency Q_{abs} as

$$k_\eta = Q_{\text{abs}} \pi r^2 \tag{10}$$

The transmissivity of radiation through a layer of gas and particles is calculated for each of the i participating gases, including soot, as [6]

$$\tau_\eta = \prod_i \exp^{-k_{\eta,i} N_i l} \tag{11}$$

where N is the number density of radiating molecules, k_η is the absorption coefficient, and l is the path length. Beer's law was used to calculate the radiance passing through a gas volume, using a black-body spectral function $B_\eta(T_{\text{vib,avg}})$ at the average molecular vibrational temperature [9],

$$T_{\text{vib,avg}} = \frac{\sum_i T_{\text{vib},i} N_i}{\sum_i N_i} \tag{12}$$

$$R_{\eta,\text{out}} = \tau_\eta R_{\eta,\text{in}} + (1 - \tau_\eta) B_\eta(T_{\text{vib}}) \tag{13}$$

where $R_{\eta,\text{out}} - R_{\eta,\text{in}}$ is the change in spectral radiance over the gas element, and $B_\eta(T)$ is the black-body source function,

$$B_\eta(T) = \frac{2hc^2\eta^3}{\exp^{c_2\eta/T} - 1} \tag{14}$$

The NERD program was written in FORTRAN 77 using a workstation running Red Hat Linux 9.0. The user specifies a wave number range and number of subintervals (e.g., wave number resolution). The program searches the database to obtain $S_\eta(T_{\text{ref}})$ and η_0 and then solves for the absorption coefficient, k_η. It treats each wave number independently, solving for its transmissivity and radiance throughout the line of sight. When this is complete, it calculates the total intensity over the specified wave number interval and the average radiance. Finally, it includes a subroutine to convolve the spectral radiance with a shape function to accurately simulate experimental measurements.

The NERD program is simple to parallelize because every wave number and line of sight is independent of all others. In the parallel message-passing interface (MPI)-FORTRAN form chosen, the wave number range is separated and assigned to a processor. The master processor begins by reading the flowfield and radiation databases into memory and then divides the wave number range to be distributed among the slave processors. Each slave processor calculates the transmissivity at each point of the flowfield for the assigned wave numbers using Eq. (11) and then calculates the radiative transport through those points with Eq. (13). The master processor then accumulates all slave processor radiance values into one data file and applies the user-specified shape function. When this is completed, the master processor integrates over the spectrum to find the intensity. Figure 1 shows the parallelization efficiency for the stated scheme. The actual run time is higher than the theoretical minimum (i.e., if all tasks were evenly distributed among processors) as the number of processors increases. The loss in efficiency is because the mandatory master processor calculations represent a larger portion of the total execution time as slave processors are added.

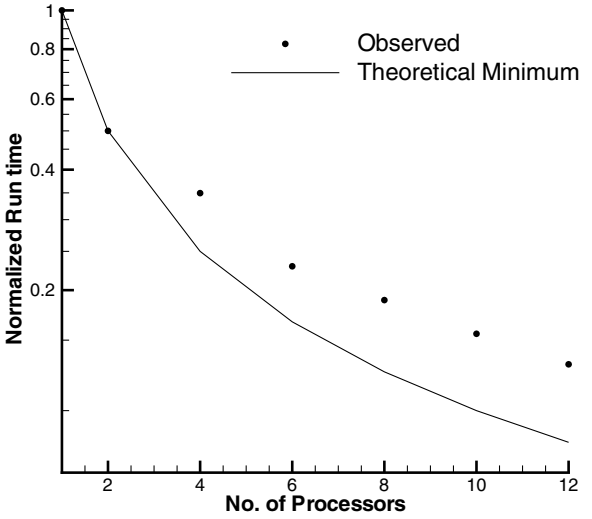

Fig. 1 A comparison of the normalized NERD run time compared to the theoretical minimum, when all tasks are evenly divided among the processors.

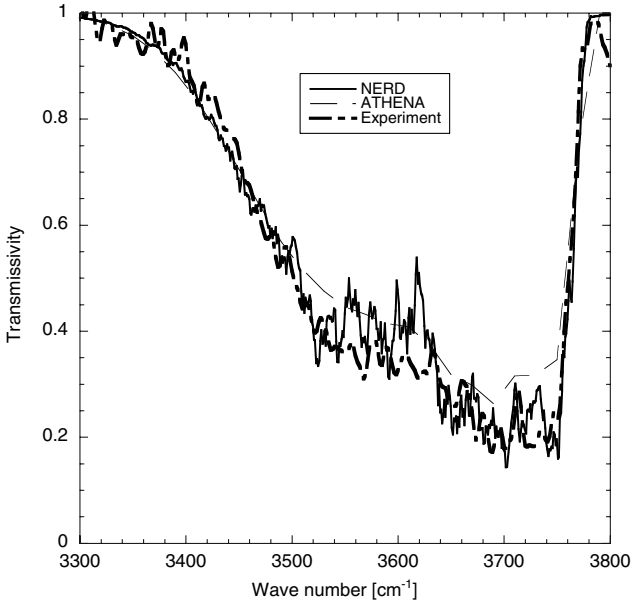

Fig. 2 Comparison of CO_2 transmissivity between NERD, ATHENA, and experiment [13] for wave numbers between 3300 and 3800 cm^{-1}. Optically thin case. $T = 1300$ K, $P = 1$ atm, $l = 20$ cm, and wave number resolution = 4 cm^{-1}.

III. Model Verification

The NERD computations have been compared with both experimental and modeled spectra. Figures 2 and 3 compare the calculated CO_2 transmissivities with data for both optically thin and optically thick cases, respectively. The transmission was derived from the absorption data of Modest [13]. In both cases, the gas has an equilibrium temperature of 1300 K, a pressure of 1 atm, and layer thicknesses L are 20 and 40 cm, respectively. NERD resolves the experimental molecular structure, thereby providing a more accurate prediction of the observed transmissivities than ATHENA for both cases.

The LTE radiance data in Figs. 2 and 3 are also compared with calculations from the ATHENA [2,14] model. The ATHENA model was used in the preflight dual-mode experiment of bow-shock interactions (DEBI) predictions [15] and for preliminary comparisons between data and calculations, because it was the only high-temperature spectral model capable of modeling shock layer radiation of polyatomic molecular systems. The ATHENA model is a narrow-band random Elasser model which is

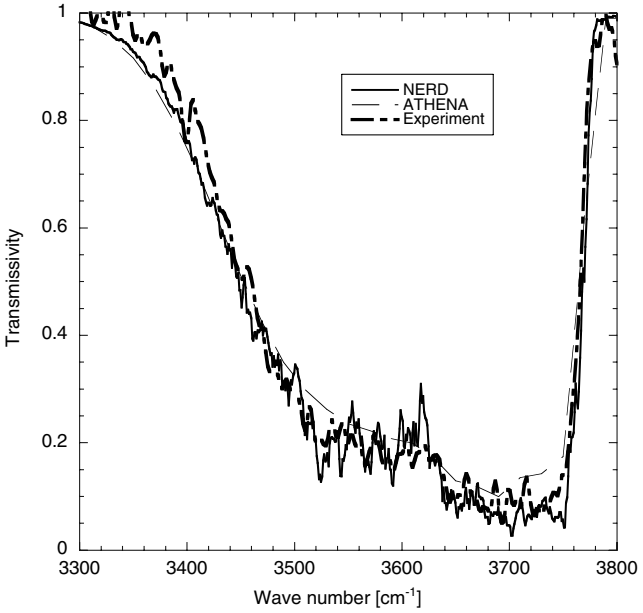

Fig. 3 Comparison of CO_2 transmissivity between NERD, ATHENA, and experiment [13] for wave numbers between 3300 and 3800 cm^{-1}. Optically thick case. $T = 1300$ K, $P = 1$ atm, $l = 40$ cm, and wave number resolution = 4 cm^{-1}.

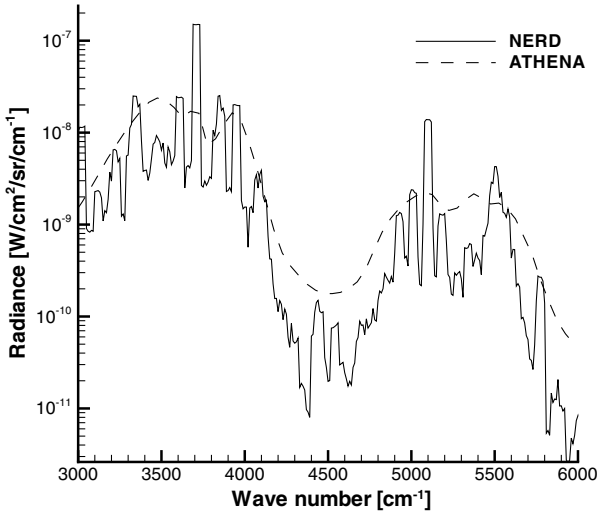

Fig. 4 Comparison of simulated spectra H_2O at 1500 K between NERD and ATHENA. $P = 0.001$ atm, $l = 1$ cm, and wave number resolution = 0.5 cm^{-1}.

computationally less demanding than a line-by-line model, but is potentially less accurate due to poorer spectral resolution. Figure 4 shows a comparison of a simulated H_2O spectra for the NERD and ATHENA models. The two models show similar values, particularly in the peak radiation regions, but NERD shows that there is wave number structure for each peak which is not captured by ATHENA [2] due to ATHENA's lower spectral resolution.

To make a direct comparison with a non-LTE model such as NEQAIR-IR [3], NERD was used to calculate high-temperature CO radiance, using the CO spectral database from HITEMP. In NEQAIR-IR the integrated intensity of a transition E_η is related to the molecular quantum mechanical parameters [16],

$$E_\eta = \frac{16\pi^3 c N_u \eta^4}{3(2J_l + 1)} |R_e(r_{v_l v_u})|^2 q_{v_l v_u} S \tag{15}$$

where N_u is the population of the upper state, $|R_e(r_{v_l v_u})|^2$ is the squared transition moment, $q_{v_l v_u}$ is the Franck–Condon factor, and S is the line intensity factor [16]. The corresponding value for NERD can be calculated with Eq. (11) and the definition of line strength from Rothman [4]

$$E_\eta = N \int_{-\infty}^{+\infty} B_\eta(T) k_\eta \, \mathrm{d}\eta = S_\eta(T) N B_\eta(T) \tag{16}$$

See [17] for more details. Equating (15) and (16), a direct comparison can be drawn between $\mathcal{R}_{lu}$ that is obtained directly from the HITRAN database and with one derived from the values of $|R_e(r_{v_l v_u})|^2$, $q_{v_l v_u}$, S, and other quantum mechanical parameters used in the NEQAIR-IR computer code.

$$\mathcal{R}_{lu} = \frac{g_u}{g_l} \frac{|R_e(r_{v_l v_u})|^2 q_{v_l v_u} S}{2J_l + 1} \tag{17}$$

The direct comparison of HITRAN and NEQAIR-IR is further complicated because their respective values of the integrated line strength intensities S_η are different. The HITRAN model bases its weighted transition-moment squared $\mathcal{R}_{lu}$ on the electron dipole-moment function from Chackerian and Tipping [18], whereas that of NEQAIR-IR is based on that from Langhoff and Bauschlicher [19]. The difference between these two electron dipole-moment functions can be seen in Table 1. Calculations of the integrated intensities for the P branch of the 3-2 vibrational transitions of CO shows NEQAIR-IR consistently reporting higher values than those given by HITRAN, especially for the lower rotation quantum numbers [17]. Figure 5 presents the calculated spectra of a 5 cm thick layer of CO at a pressure of 1 atm. The spectra were first computed for an equilibrium gas at a temperature of 1000 K and then the translational, rotational, and vibrational temperatures were separately increased to 1500 K (Trans, Rot, and Vib on the figure) with all other temperatures remaining at 1000 K. The figure shows that both programs show similar nonequilibrium behavior as the temperatures are changed and the difference in the magnitude of the radiation is related to the aforementioned transition of moments. Note that the reason that the intensity increases when the vibrational temperature is set to 1500 K, while the other temperature values remain at 1000 K, is because the higher vibrational temperature increases the upper vibrational state population. The average discrepancy between NERD and NEQAIR-IR for all cases, except vibrational excitation, is 10%. NERD and NEQAIR-IR differ by 30% when the vibrational temperature was increased.

Table 1 Comparison of rotationless matrix elements from electron dipole-moment functions used in HITRAN and NEQAIR

Rotationless matrix elements, D	NEQAIR [19]	HITRAN [18]
$M_0^0(0)$	-0.1117	-0.10982
$M_0^1(0)$	0.1077	0.1084
$M_0^2(0)$	-6.53×10^{-3}	-6.6×10^{-3}
$M_0^3(0)$	4.14×10^{-4}	4.29×10^{-4}
$M_0^4(0)$	-2.24×10^{-5}	-2.016×10^{-5}

Finally, we considered the validation of our pseudogas particle radiation model with the sooting diffusion flame studied by Santoro. In his work [20], the experimentally measured extinction coefficients k_{ext} and scattering measurements were used to calculate soot radius and number density using the Rayleigh theory for scattering and absorption of light from spherical particles. The extinction coefficient is defined such that the ratio of outgoing laser probe intensity I to incoming laser radiance I_0 is

$$\frac{I}{I_0} = \exp\left(- \int k_{\text{ext}} \, \mathrm{d}x \right) \tag{18}$$

Since $\frac{I}{I_0}$ is the transmissivity of the laser light, Eq. (18) may be combined with Eq. (11) to give

$$k_{\text{ext}} = Q_{\text{ext}} N \pi r^2 \tag{19}$$

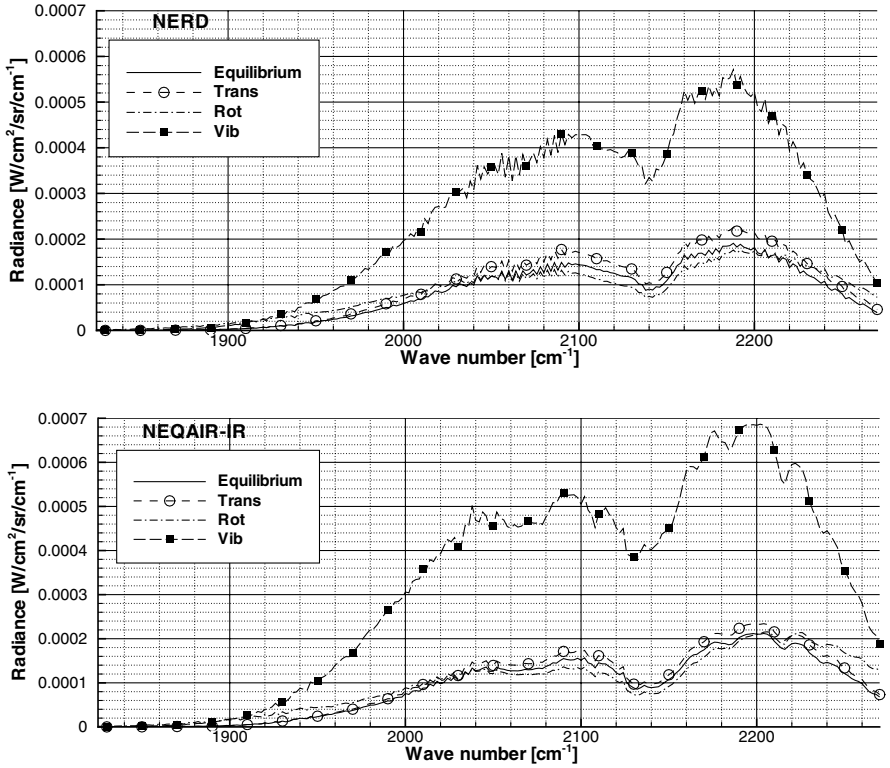

Fig. 5 Comparison of NERD (above) and NEQAIR (below) CO radiance as each temperature is excited from 1000 to 1500 K. Wave number resolution = 0.1 cm^{-1} for all simulations.

Values of number density N and soot radius r obtained from Santoro [20] were used in NERD to calculate Q_{ext} and k_{ext}. Measurements were taken along horizontal, radial slices of the flame at different heights, with $x = 0.3$ in. corresponding to the flame axis. The extinction coefficients derived from the data of Santoro [20] and the NERD predictions are shown in Fig. 6 for two heights in the flame. Although both conditions agree closely, discrepancies are evident in the central region of the flame for the 50 mm case. There are two possible sources of errors that can contribute to this discrepancy. One is that there is a maximum error of about 15% in the measurements of the soot volume fraction,* which contributes proportionally to the error in the extinction coefficient. The second is that the discrepancy between modeled values and observed data could also be due to the assumption in [20] that the particle sizes follow a self-preserving particle size distribution function, while we have assumed a uniform particle size in a discretized volume of gas. However, most importantly, the modeled and measured numbers are very similar in the highly radiative shear layer.

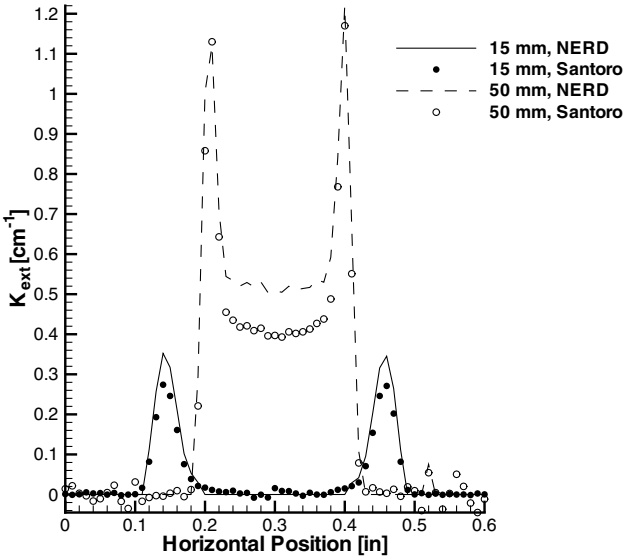

Fig. 6 Comparison of NERD simulation of the extinction coefficient k_{ext} of a diffusion flame measured by Santoro at two different heights above the flame base.

IV. Applications of the NERD Radiation Model

A. DEBI Bow-Shock Experiment

The DEBI [15] consisted of forward- and side-looking spectrometers mounted in the nose cone of a sounding rocket that was launched from Wallops Island in 2003. The reduction of the experimental data is incomplete and not available for comparison with modeling and simulation. However, because the ability to accurately model hypersonic shock layer radiation is important for many space applications, spectra predicted by NERD are presented here. Figures 7 and 8 show the flowfield temperatures and species concentrations along the stagnation streamline for the DEBI shape [15].

Figure 9 shows the calculated spectra for freestream conditions of 40 km and 3.5 km/s, with CO_2 and H_2O radiance calculated by NERD and all other values calculated by NEQAIR-IR. The calculations presented here used a rectangular shape function with a width of 40 cm^{-1} to simulate the onboard spectrometer. The strong CO_2 overtones, seen as peaks at 2300, 3800, and 5000 cm^{-1}, indicate that it is the predominant radiator in the flow, while H_2O contributes to the radiance between the peaks. Comparison of Fig. 9 with the earlier spectra computed by ATHENA in [15] shows similar magnitudes but small variations in the band shapes, which is expected because ATHENA neglects the nonequilibrium features of the gas.

B. Atlas Plume Radiation

The second example that we considered is the high-temperature spectra from a two-phase flow underexpanded, rocket plume. In the

*Santoro, R. J., personal communication [11 April 2005].

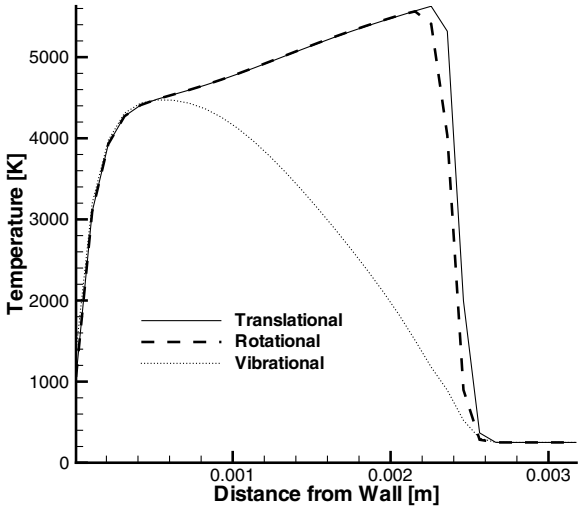

Fig. 7 Modeled CO_2 translational, rotational, and vibrational temperatures along the stagnation streamline of the DEBI sounding rocket for freestream conditions corresponding to 40 km altitude and a velocity of 3.5 km/s.

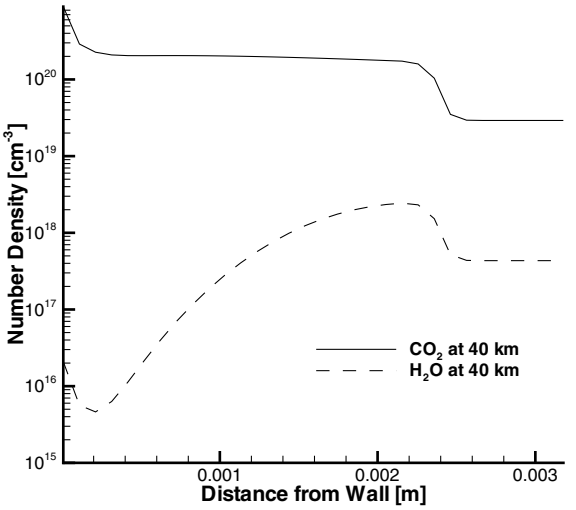

Fig. 8 Calculated species concentration along the stagnation streamline for the DEBI experiment.

work of Viswanath et al [10], the modeling of soot combustion in the flowfield of a single-nozzle Atlas rocket plume was investigated. The molecular flowfield was represented by a third order accurate converged Navier–Stokes solution for a chemically reacting gas flow using the GASP CFD code [21]. The high Reynolds number κ–ϵ turbulence model was used to improve the characterization of the plume shear layer. The freestream conditions corresponded to those at 21 and 40 km, assuming that the plume flow started at the nozzle exit, that is, the rocket-body plume interaction was ignored. A continuum soot field was overlayed on the molecular flowfield with the assumption that the soot volume fraction is sufficiently small so that the macroscale flowfield is not affected. A soot particle mass fraction of 0.5% was assumed giving a number density of 7.8×10^{14} particles/m^3 and an initial particle radius of 50 nm at the nozzle exit. Oxidation of the soot particles was incorporated into the calculation using the Heirs's oxidation model [22], although condensation and agglomeration were neglected. The oxidation process was represented as a reduction in particle radius with time $\frac{dr}{dt}$, while preserving the number density of soot particles.

The axisymmetric flowfield was swept into a 3-D rectilinear grid with a resolution of 0.4 m in every direction, which could be further broken into a 2-D image of 1-D lines of sight. The radiative intensities of soot, CO_2 and H_2O, were calculated for two bands:

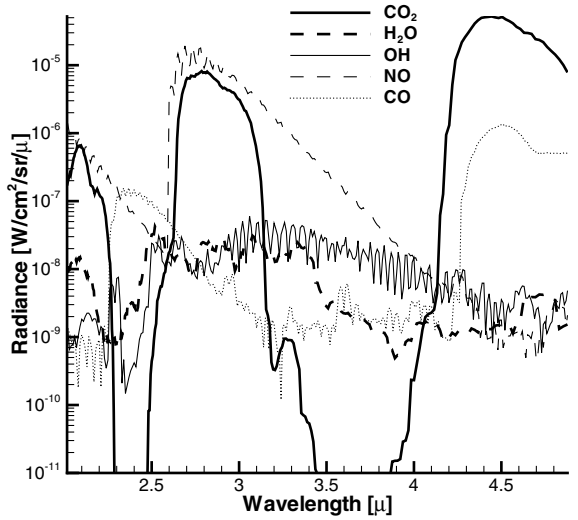

Fig. 9 Modeled spectra from the forward-looking DEBI spectrometer at 40 km using NERD with a wavelength resolution of 0.0005 μ. CO, NO, and OH radiation was calculated using NEQAIR-IR.

3.91–4.00 μ, which is dominated by soot radiation, and 4.67–4.81 μ, which is at the peak of the CO_2 fundamental.

Viswanath's results [10] predict a 0.7% reduction in average particle radius due to oxidation for the first 100 m of the plume at 21 km and only 0.1% for the 40 km solution. Plume images were simulated with NERD at 21 km using the same two-phase flowfields of Viswanath et al. [10]. A comparison of the simulated infrared images, with and without oxidation, did not reveal any significant difference [17]. This suggests that either more chemical reactions need to be added to the oxidation model or that soot combustion plays a small role in plumes compared to agglomeration and particle fracture.

Full radiation signatures of the plume at 21 and 40 km for both bands discussed above can be found in Figs. 10–13. The Atlas flowfield computation was interpolated with a spatial resolution of 0.4 m and a spectral resolution of about 0.2 cm^{-1} with a rectangular shape function of 500 Å used for all cases. In each figure, the lower contour is modeled assuming soot radiation only, the middle contour shows molecular radiation only, and the upper contour shows the

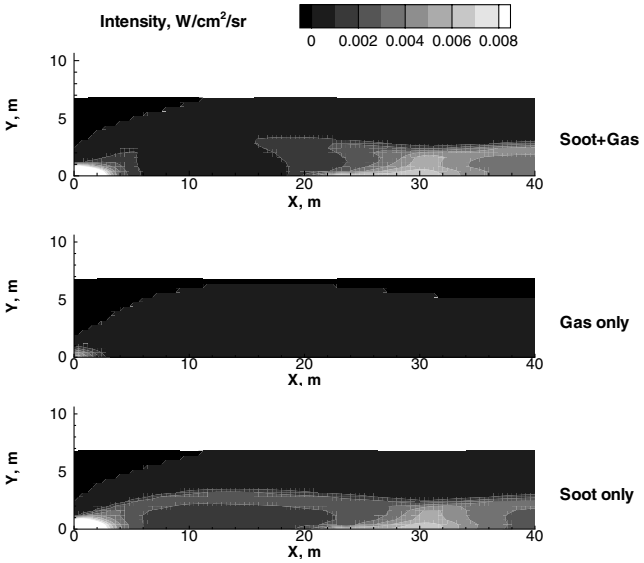

Fig. 10 Simulated infrared radiation image from an Atlas booster at 21 km in the 3.91–4.00 μ band. This is shown in three elements: soot radiation (lower), gas radiation (middle), and a mixture of both (top). The maximum intensity in the plot is 0.1012 W/cm^2 · sr and appears at the nozzle exit of the soot + gas case.

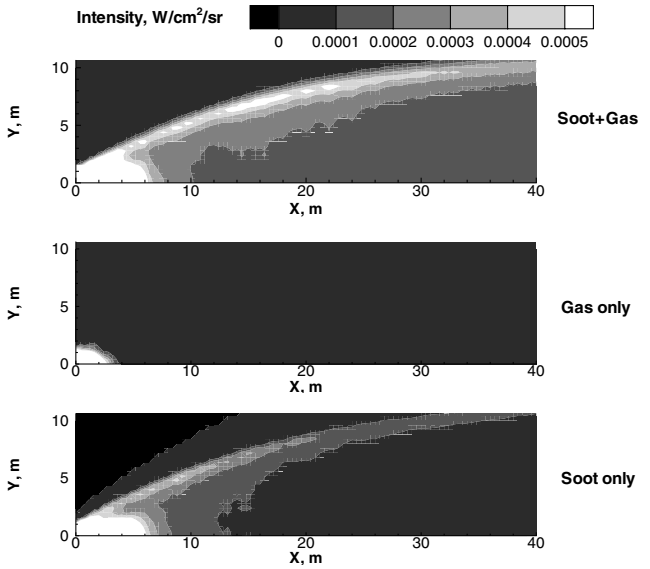

Fig. 11 Simulated infrared radiation image from an Atlas booster at 40 km in the 3.91–4.00 μ band. This is shown in three elements: soot radiation (lower), gas radiation (middle), and a mixture of both (top). The maximum intensity in the plot is 0.0390 W/cm^2 · sr and appears at the nozzle of the soot + gas case.

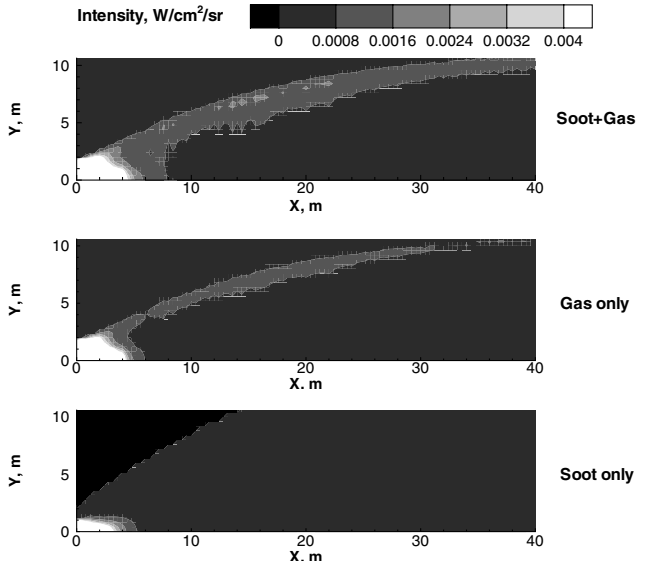

Fig. 13 Simulated infrared radiation image from an Atlas booster at 40 km in the 4.67–4.81 μ band. This is shown in three elements: soot radiation (lower), gas radiation (middle), and a mixture of both (top). The maximum intensity in the plot is 0.2187 W/cm^2 · sr and appears at the nozzle of the soot + gas case.

radiation when both are present. The contour maximum is set below the maximum intensity value, flooding the contour at the upper levels, to reveal extra details in the simulated images. As expected, the radiation was brighter in the 4.67–4.81 μ band because it was located on the CO_2 fundamental frequency. In addition, the radiation was also brighter for the 21 km solution due to a higher concentration of both molecular and particulate radiators. It was observed that the highest intensity for each case can be found at the nozzle exit and then the shear layer. Because the plume is shorter at 21 km, the barrel shock is also observed in Figs. 10 and 12. The residual structure observed in the 40 km simulated images is due to the finite spatial resolution of the original CFD calculations of 0.1 m compared to the large gradients in the thin shear layer.

Figures 14 and 15 show the spectral intensity of the Atlas plume at 21 and 40 km, integrated spatially over the first 100 m of the flowfield. The spatial resolution was 1.0 m and the spectral resolution

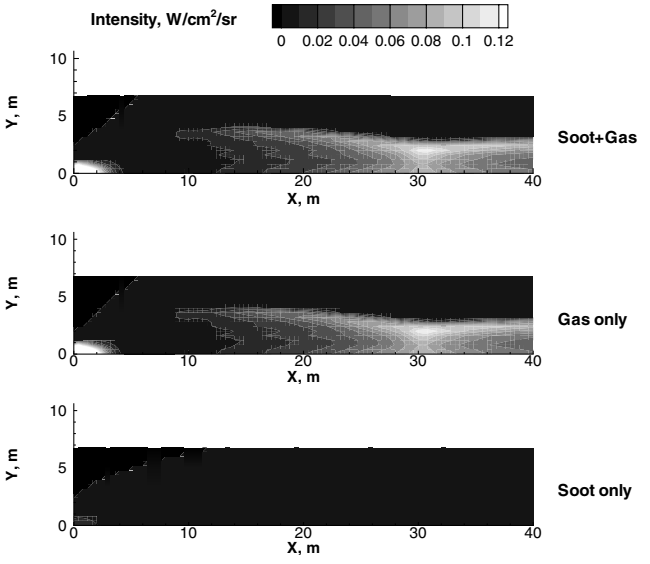

Fig. 12 Simulated infrared radiation image from an Atlas booster at 21 km in the 4.67–4.81 μ band. This is shown in three elements: soot radiation (lower), gas radiation (middle), and a mixture of both (top). The maximum intensity in the plot is 0.2283 W/cm^2 · sr and appears at the nozzle of the soot + gas case.

was 0.0045 μ. The gas temperature averaged over the first 100 m of the flow is similar for the two altitudes: 720 and 520 K, at 21 and 40 km, respectively. However, the average pressure is approximately an order of magnitude higher for the 21 km spectra. The difference in peak shape between the two spectra is primarily due to the greater pressure broadening at 21 km. Each plot includes two spectra: one calculated assuming molecular radiation only, the other fully incorporating soot and molecular emission and absorption. This allows a good assessment of the impact soot has on the radiation of the plume. The CO_2 fundamental band is clearly evident at 4.5 μ, with the serrated form of the H_2O peaks only appearing in the 2.5–3.0 μ wavelength region. The addition of soot to the flowfield increases the intensity especially in the 2.0–2.5 μ region. The increase is more noticeable as the wavelength shortens because the soot particles become more efficient emitters. Inclusion of particle radiation does not noticeably increase the radiation in the 4.5 μ CO_2 band because the gaseous flowfield is already optically thick.

In earlier work, Alexeenko et al. [23] analyzed similar spectral cases, but for a larger mass flow, larger mass fraction of soot, and a three nozzle Atlas nonaxisymmetric geometry. It was found that the spectra were similar to those presented here, but the larger mass

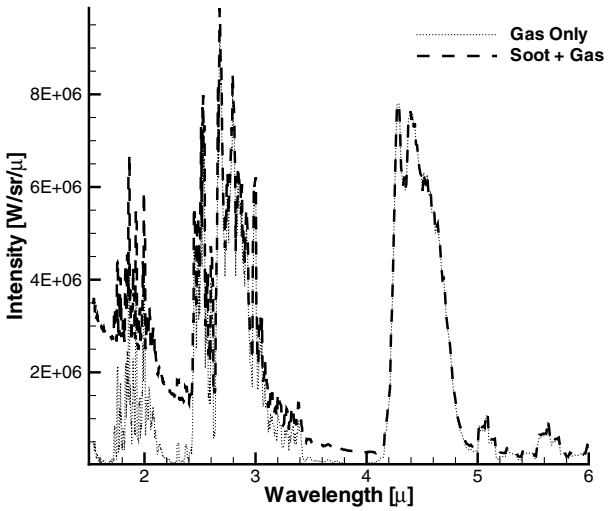

Fig. 14 The spatially integrated intensity of simulated infrared radiation in the Atlas plume at 21 km altitude.

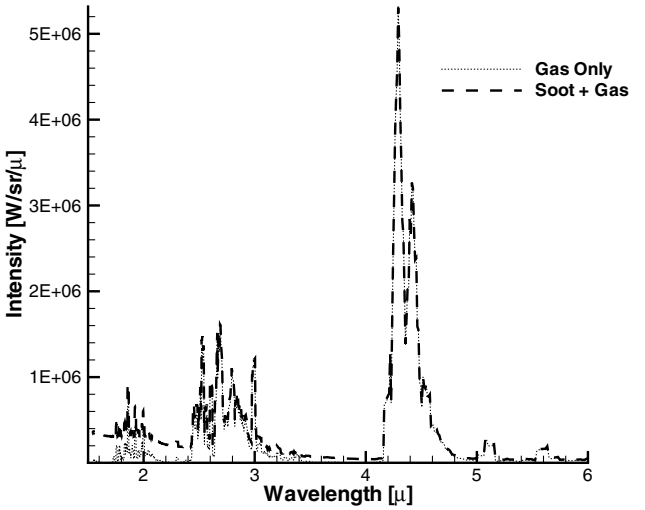

Fig. 15 The spatially integrated intensity of simulated infrared radiation in the Atlas plume at 40 km altitude.

fraction of soot resulted in greater molecular peak reabsorption than was observed in this work. In addition, it was also found that the larger mass fraction of soot increased the radiation between peaks more than was seen here. Therefore the specific effects of soot particulates on the overall plume radiation depends on the nature of the two-phase plume flow.

V. Conclusions

In this paper, we have presented the development of NERD, a complex radiation simulation to be used in determining the infrared image and spectral distribution of radiation from high-temperature flowfields. Gaseous radiation is calculated using a line-by-line approach with the CDSD-1000 and HITRAN/HITEMP databases. Nonlocal thermal equilibrium effects are modeled by separation of the internal partition sums and dividing the molecular state energies into their vibrational and rotational components. The particulate radiation problem is simplified because the soot radius sizes considered in the Atlas application are not large compared to the wavelengths of light considered. Therefore the Mie theory for scattering can be simplified by the first-term approximation. Furthermore, the small particle size implies that nearly all of the extincted photons are absorbed instead of scattered, allowing the application of the pseudogas assumption. Finally, the program was parallelized using MPI-FORTRAN 77 to be run on cluster computers.

The NERD model was tested for two applications. For the first application, the shock-heated infrared spectrum resulting from gases in the highly nonequilibrium stagnation region of a hypersonic vehicle was obtained. The output for CO_2 and H_2O was combined with diatomic results from NEQAIR to form a full spectrum. In the second application, the image of a two-phase flowfield consisting of soot and gas within the plume of an Atlas rocket at different wave number bands was obtained. The results showed that the earlier predicted soot combustion is insufficient to affect the radiation signature of the plume. Full infrared images of the plume were generated at 21 and 40 km for two bands, with each image being divided into its molecular and particulate components.

The present particle radiation formulation in NERD is not sufficiently general to accommodate a wider variety of particle sizes. As they grow in size, both the pseudogas assumption and first-term approximation become invalid. The latter problem can be addressed by adding the second and third terms of the Mie theory into the model. However, invalidating the pseudogas assumption requires the incorporation of scattering into the model. In this case, the radiation environment at each point is dependent on every other point in the flowfield, which greatly complicates the parallel computation scheme.

Acknowledgments

This work was supported by the Army Research Office Grant No. DAAD19-02-1-0196, administered by David Mann. The authors wish to express their gratitude to M. F. Modest and R. J. Santoro for their help in using their data, and DAL would like to thank Kenneth Schwartz of DTRA for his assistance in obtaining technical documentation for the ATHENA model. Special thanks go to J. Devore, R. J. Santoro, and M. F. Modest for their technical discussions and suggestions. Finally, we acknowledge the Navier–Stokes CFD solutions calculated by Michael Wright of NASA/Ames Research Center for the DEBI shape at 40 km.

References

[1] Park, C., "Nonequilibrium Air Radiation (NEQAIR) Program: Users Manual," Ames Research Center, NASA, 1985.

[2] Devore, J., "ATHENA User's Guide," TM, Physical Research, Inc., Sept. 1987.

[3] Packan, D., Laux, C. O., Gessman, R. J., Pierrot, L., and Kruger, C. H., "Measurement and Modeling of OH, NO, and CO Infrared Radiation at 3400 K," *Journal of Thermophysics and Heat Transfer*, Vol. 17, No. 4, 2003, pp. 450–456.

[4] Rothman, L. S., Rinsland, C. P., Goldman, A., Massie, S. T., Edwards, D. P., Flaud, J. M., Perrin, A., Camy-Peyret, C., Dana, V., and Mandin, J. Y., Schroeder, J., Mccann, A., Gamache, R. R., Wattson, R. B., Yoshino, K., Chance, K. V., Jucks, K. W., Brown, L. R., Nemtchinov, V., and Varanasi, P., "The HITRAN Molecular Spectroscopic Database and HAWKS (HITRAN Atmospheric Workstation): 1996 Edition," *Journal of Quantitative Spectroscopy and Radiative Transfer*, Vol. 60, No. 5, 1998, pp. 665–710.

[5] Tashkun, S. A., Perevalov, V. I., Teffo, J-L., Bykov, A. D., and Lavrentieva, N. N., "CDSD-1000, the High-Temperature Carbon Dioxide Spectroscopic Databank," *Journal of Quantitative Spectroscopy and Radiative Transfer*, Vol. 82, No. 1, 2003, pp. 165–196.

[6] Ludwig, C. B., Malkmus, W., Reardon, J. E., and Thompson, J. A. L., "HandBook of Infrared Radiation from Combustion Gases," NASA SP-3080, Scientific and Technical Information Office, Washington, D.C., 1973.

[7] Herzberg, G., *Molecular Spectra and Molecular Structure II: Infrared and Raman Spectra of Polyatomic Molecules*, 9th ed., D. Van Nostrand Company, Princeton, NJ, 1945.

[8] Ludwig, R., and Weinhold, F., "Quantum Cluster Equilibrium Theory of Liquids: Light and Heavy QCE/3-21G Model Water," *Physical Chemistry Chemical Physics*, Vol. 2, March 2000, pp. 1613–1619.

[9] Modest, M. F., *Radiative Heat Transfer*, 2nd ed., Academic Press, New York, 2003.

[10] Viswanath, K., Brentner, K. S., Gimelshein, S. F., and Levin, D. A., "Investigation of Soot Combustion in Underexpanded Jet Plume Flows," *Journal of Thermophysics and Heat Transfer*, Vol. 19, No. 3, 2005, pp. 282–293.

[11] Plastinin, Y. A., Karabadzhak, G. F., Khmelinin, B. A., Baula, G. G., and Rodionov, A. V., "Modeling of OH Ultraviolent Radiation in Atlast Motor Plume and Comparison with Recent Experimental Data," AIAA Paper 2003-507, Reno, NV, 2003.

[12] Kim, C., Lior, N., and Okuyama, K., "Simple Mathematical Expression for Spectral Extinction and Scattering Properties of Small Size-Parameter Particles, Including Examples for Soot and TiO_2," *Journal of Quantitative Spectroscopy and Radiative Heat Transfer*, Vol. 55, No. 3, 1996, pp. 391–411.

[13] Modest, M. F., and Bharadwaj, J., "Medium-Resolution, High-Temperature Transmissivity Measurements and Correlations for Carbon Dioxide-Nitrogen Mixtures," *Journal of Quantitative Spectroscopy and Radiative Transfer*, Vol. 73, No. 2–5, 2002, pp. 329–338.

[14] Stephens, T. L., Stull, V. R., Klein, A. L., and Losse, J. D., "The ROSCOE Manual," *Molecular Band Models for Thermal and Optically-Pumped Emissions*, Vol. 28, Center for Advanced Studies, General Electric Company, Santa Barbara, CA, 1978.

[15] Levin, D. A., Candler, G. V., and Limbaugh, C. C., "Multispectral Shock-Layer Radiance from a Hypersonic Slender Body," *Journal of Thermophysics and Heat Transfer*, Vol. 14, No. 2, 2000, pp. 237–243.

[16] Arnold, J. O., Whiting, E. E., and Lyle, G. C., "Line by Line Calculation of Spectra From Diatomic Molecules and Atoms Assuming a Voigt Line Profile," *Journal of Quantitative Spectroscopy and Radiative Transfer*, Vol. 9, No. 6, 1969, pp. 775–798.

[17] Garrison, M. B., Ozawa, T., and Levin, D. A., "An Improved Radiation Model for CO_2, H_2O and Soot in High-Temperature Flows," AIAA Paper 2005-4777, Toronto, 2005.

[18] Chackerian, C., and Tipping, R. H., "Vibration-Rotational and Rotational Intensities for CO Isotopes," *Journal of Molecular Spectroscopy*, Vol. 99, No. 2, 1983, pp. 431–449.

[19] Langhoff, S. R., and Bauschlicher, C. W., "Global Dipole Moment Function for the Ground State of CO," *Journal of Chemical Physics*, Vol. 102, No. 13, 1995, pp. 5220–5225.

[20] Santoro, R. J., Semerjian, H. G., and Dobbins, R. A., "Soot Particle Measurements in Diffusion Flames," *Combusion and Flame*, Vol. 51, 1983, pp. 203–218.

[21] GASP Ver. 3, The General Aerodynamic Simulation Program, Computational Flow Analysis Software for the Scientist and Engineer, User's Manual, Aerosoft Co., Blacksburg, VA, May 1996.

[22] Heirs, R. S., III, "Rarefaction Effects in Small Particle Combustion," Ph.D. Thesis, University of Tennessee, Aug. 1997.

[23] Alexeenko, A. A., Gimelshein, N. E., Levin, D. A., Collins, R. J., Rao, R., Candler, G. V., Gimelshein, S. F., Hong, J. S., and Schilling, T., "Modeling of Flow and Radiation in the Atlas Plume," *Journal of Thermophysics and Heat Transfer*, Vol. 16, No. 1, 2002, pp. 50–57.